

Experimental study of two-proton correlated emission from ^{29}S excited states

C. J. Lin,* X. X. Xu, H. M. Jia, F. Yang, F. Jia, S. T. Zhang, Z. H. Liu, and H. Q. Zhang
China Institute of Atomic Energy, Beijing 102413, People's Republic of China

H. S. Xu, Z. Y. Sun, J. S. Wang, Z. G. Hu, M. Wang, R. F. Chen, X. Y. Zhang, C. Li,
 X. G. Lei, Z. G. Xu, G. Q. Xiao, and W. L. Zhan
Institute of Modern Physics, The Chinese Academy of Science, Lanzhou 73000, People's Republic of China
 (Received 11 December 2008; revised manuscript received 29 March 2009; published 13 July 2009)

An experiment of a ^{29}S beam bombarding a ^{197}Au target at an energy of 49.2 MeV/u has been performed to study the two-proton correlated emission from ^{29}S excited states. Complete-kinematics measurements were carried out in the experiment. The relative momentum, opening angle, and relative energy of two protons, as well as the invariant mass of the final system, were deduced by relativistic-kinematics reconstruction. The ^{27}Si - p - p coincident events were picked out under strict conditions and the phenomenon of p - p correlations was observed among these events. The mechanisms of two-proton emission were analyzed in a simple schematic model, in which the extreme decay modes like ^2He cluster emission, three-body phase-space decay, and two-body sequential emission were taken into account. Associated with the Monte Carlo simulations, the present results show that two protons emitted from the excited states between 9.6 MeV and 10.4 MeV exhibit the features of ^2He cluster decay with a branching ratio of $29_{-11}^{+10}\%$.

DOI: [10.1103/PhysRevC.80.014310](https://doi.org/10.1103/PhysRevC.80.014310)

PACS number(s): 23.50.+z, 25.60.-t, 25.70.-z, 27.30.+t

I. INTRODUCTION

One-proton ($1p$) radioactivity and two-proton ($2p$) radioactivity were proposed almost five decades ago for the proton-rich nuclei near the drip line [1,2]. One-proton radioactivity was first observed experimentally at the beginning of the 1980s [3,4]. Up to now, about 25 nuclei have been found in experiments [5]. For $2p$ radioactivity, the decay mechanism becomes more complicated. Simply speaking, the $2p$ events detected in the experiment may root in three ways: (i) two-body sequential emission in a short time, (ii) three-body simultaneously democratic emission [6], and (iii) ^2He cluster emission and then breakup. Two protons in a ^2He cluster are basically constrained by the pair correlation in a quasibound s singlet, i.e., ^1S configuration. The Coulomb barrier can guarantee the existence of such a quasibound state for an instant. After penetration of the barrier, the two protons will be separated. (see Fig. 1 in Ref. [5] for reference). The experimental search for the $2p$ emitter started very early [6,7], and many nuclei [8–22] have been investigated, but more precise experiments and modern theories are still required to comprehensively understand the decay mechanism. The current progress of experiment and theory on $2p$ radioactivity can be found in a recent review paper, Ref. [5].

In general, a halo/skin structure may occur [23,24] when $2p$ are close to the threshold. At this moment, the interaction between valence particles and the core becomes weak while the correlation between two protons correspondingly becomes strong. When the nucleus is excited, $2p$ may have a large spectroscopic factor to populate at a certain level above the threshold and lead to direct decay [5,25,26]. The ^{29}S nucleus ($Z = 16$), two valence protons, which locate in the $2s_{1/2}$ orbit

with a binding energy of 5.35 MeV, may have such an exotic behavior. An obvious enhancement in the total reaction cross section of $^{29}\text{S} + ^{28}\text{Si}$ at intermediate energy has been reported [27], indicating the possibility of $2p$ halo/skin in ^{29}S . Later, the experimental signatures of $2p$ emission were observed in the $^{29}\text{S} + ^{12}\text{C}$ reaction [28]. In this article, we present new experimental results to show the evidences of $2p$ correlated emission from the ^{29}S excited states.

II. EXPERIMENTAL PROCEDURE**A. Experimental setup**

The experiment was performed at HIRFL-RIBLL [29] of the Institute of Modern Physics, Lanzhou. The secondary ^{29}S beam with an energy of 49.2 MeV/u was produced by the projectile fragmentation of a primary ^{32}S beam bombarding a 1.59-mm-thick ^9Be target at 80.4 MeV/u. A homogeneous ^{27}Al degrader with a thickness of 490 μm was used to purify the secondary beam. The typical current of the primary beam was 100 enA, producing the secondary beam with a total intensity about 10^4 ions/sec. Two scintillator detectors were placed in the T1 and T2 target chambers of the RIBLL spectrometer, respectively, to generate the time-of-flight (ToF) signals of secondary heavy ions. The whole detector array was emplaced in the T2 chamber to perform the complete-kinematics measurements with which all the decay products were detected. The experimental setup of the detector array is plotted in Fig. 1.

Two PPACs with collimators (40 and 30 mm in diameter, respectively) were located upstream of the target for beam tracking. A large area silicon detector (ΔE) was employed as the tagging detector to provide the ΔE signals. A 100- μm -thick ^{197}Au foil with a diameter of 30 mm was used as the

* cjlin@ciae.ac.cn

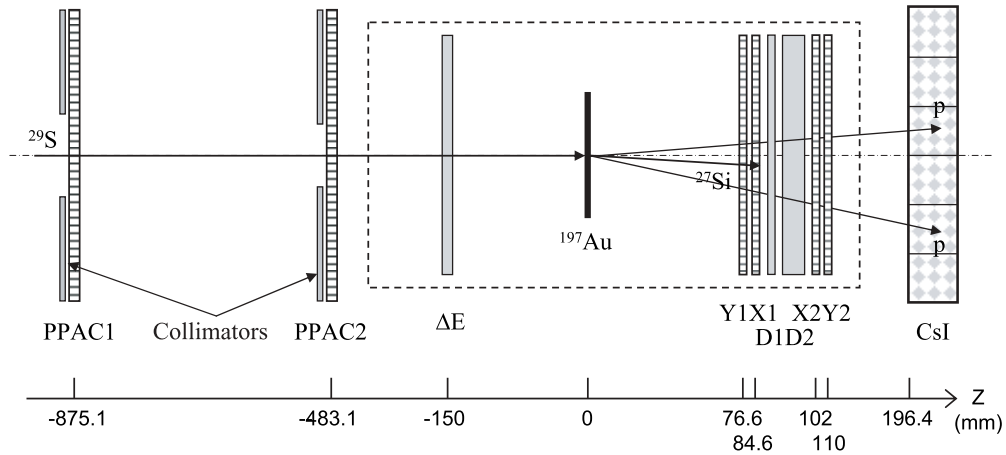


FIG. 1. Schematic plot of experimental setup for complete-kinematics measurements. The direction of the beam was defined as the Z axis. The positions of the detectors relative to the target are denoted in the bottom scale.

secondary reaction target. Two orthogonal Single-sided Silicon Strip Detectors (SSSDs) with a thickness of $300\ \mu\text{m}$ were placed downstream for detecting the energies, timings, and positions (Y1, X1) of the outgoing heavy fragments. Each SSSD contained 24 strips 2 mm in width and 0.1 mm in interval. A $325\text{-}\mu\text{m}$ -thick silicon detector (D1) followed the SSSDs to stop all the heavy fragments. After that, a quadrant silicon detector (D2) with a thickness of 1 mm was used to bring about the ΔE signals of light particles such as p, $2p$, etc. Another two SSSDs of the same type were employed to determine the positions (X2, Y2) of the outgoing light particles. At the end, a CsI(Tl) crystal array with 6×6 lattices was used to stop all the light particles. Every CsI(Tl) crystal has an active area of $15 \times 15\ \text{mm}^2$ with a length of 2 cm, coupling to the PIN photodiode for reading out.

The X-Y coordinates of interaction points on the target were reconstructed by two PPAC tracking detectors on the basis of the event-by-event analysis. The combination of Y1, X1, and D1 detectors and D2, X2, Y2, and CsI(Tl) detectors composed the telescopes for the reaction products of heavy fragments and light particles, respectively. The whole detector array covered $0.33\ \text{sr}$ of forward solid angle with the maximum opening angle of $\pm 13.2^\circ$ in both X and Y directions. Monte Carlo (MC) simulations showed that the detection efficiencies for the coincident ^{27}Si - p - p events were about 57.7, 57.1, and 55.5% for the ^2He cluster, three-body phase-space, and two-body sequential decay, respectively.

B. Detector calibration and beam identification

Before the formal experiment, ^{32}S beams at energies of 52.7 and 35.7 MeV/u derived from the passage of the primary beams through the ^9Be targets with thicknesses of 1.59 and 2.63 mm, respectively, were delivered to calibrate the ToFs, energies, and positions of heavy fragments by elastic scatterings. Moreover, proton beams at energies of 26, 46, 66, and 80 MeV originated from the projectile fragmentation were transported to calibrate the energies and positions of light particles. After calibrations, the RIBLL spectrometer was tuned for setting and optimizing

the ^{29}S beam. The ΔE -ToF technique was utilized to identify the ions in the secondary beam. Figure 2 illustrated the ΔE versus ToF matrix for the ion identification. The ΔE resolution became worse (about 10%) because of the large capacitance of the detector and the high intensity of the secondary beam. The purity of ^{29}S in the secondary beam was about 3%, and $2.5 \times 10^{7,29}\text{S}$ ions accumulated during the experiment.

C. Product identification

The identification of heavy products was realized mainly by the ΔE -E spectrum obtained by the Y1-X1-D1 detector combination. Figure 3 shows the Y1 versus X1 spectrum for the isotope identification after the target, which was directly generated by the elastic scatterings of the secondary beam. The closure line in the figure shows the gate for Si isotopes. Although the timing signals generated by Y1 and X1 detectors do not have adequate time resolution (about 1 ns) to identify the product masses, they are practically useful for removing

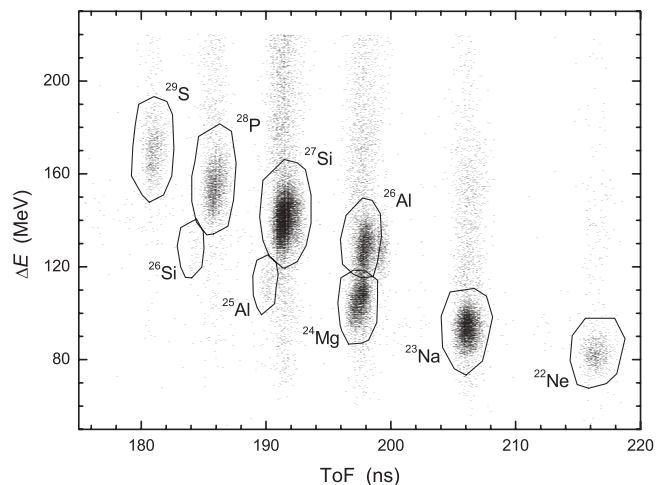


FIG. 2. Two-dimensional ΔE -ToF matrix for the identification of the secondary beam.

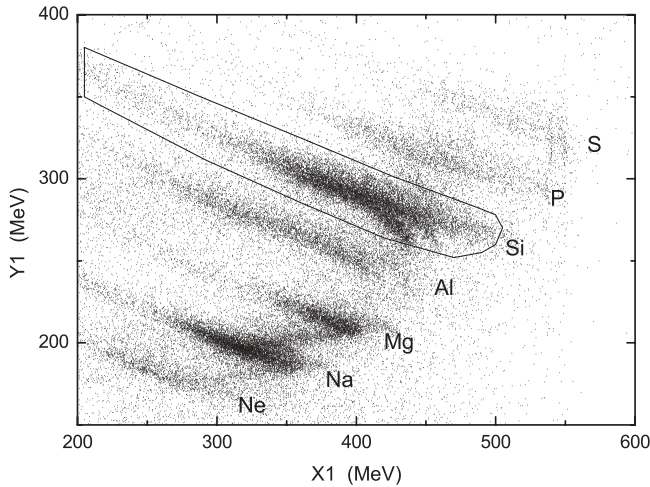


FIG. 3. Y1 versus X1 spectrum for the isotope identification of heavy products. The closed curve shows the Si-isotope band.

the accidentally coincident events and rejecting the isotope contaminations directly from the beam. A typical ToF-Y1 versus ToF spectrum is shown in Fig. 4. Here ToF-Y1 stands for the time-of-flight from the T1 scintillator detector to the Y1-SSSD after the target. ToF-Y1 is estimated to be about 10.2 ns longer than ToF. The closed curve shown in the figure indicates the time window for the ^{29}S beams and their products such as ^{28}P , ^{27}Si , etc. Some accidentally coincident events can be seen outside the time window. Combined with the ΔE - E identification, the valueless events can be rule out. For example, the $^{26,27}\text{Si}$ nuclei directly coming from the secondary beam can be rejected from the Si-isotope band in the ΔE - E spectrum by gating on a narrow time window. In this way, the interesting ^{27}Si products were scored for further analysis.

The light products were identified by the D2-X2-Y2-CsI detector combination through the ΔE - E technique, as shown in Fig. 5. The top and bottom panels show the single-hit and double-hit events, respectively, induced by the ^{29}S beam. The

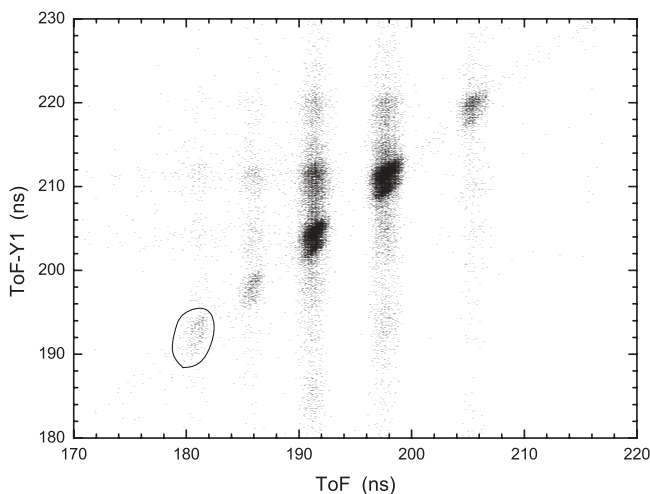


FIG. 4. ToF-Y1 versus ToF spectrum for the timing identification of heavy products. The closed curve shows the time window for the ^{29}S beams and their products.

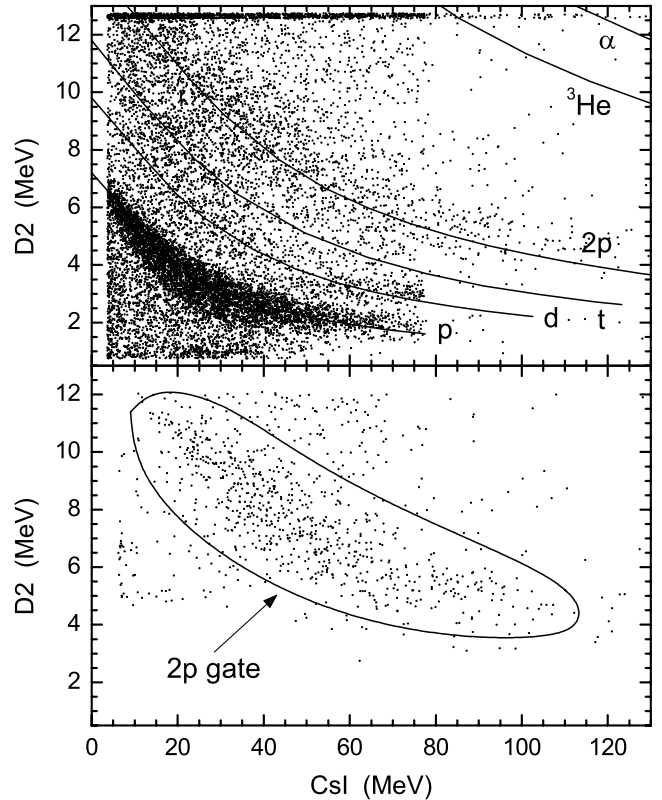


FIG. 5. D2 versus CsI spectrum for the light particle identification. The top and bottom panels show the single-hit and double-hit events, respectively, gated on ^{29}S events. The theoretical curves for different particles are shown in the top panel for reference. The closed curve in the bottom panel shows the gate for $2p$ events.

theoretical curves of p , d , t , $2p$, ^3He , and α are shown in the top panel for reference. The $2p$ events locate within a band in which the energies of both ΔE and E are two times those of the $1p$ events. A gate, shown as the closure curve in the bottom panel, was made to select the $2p$ events.

D. Trajectory tracking

The trajectories of the incoming beams and the outgoing light particles can be reconstructed by the two tracking PPACs before the target and the X2-Y2 SSSDs along with CsI array after the target, respectively. A simple “cross-point-of-trajectories method” was employed to determine the reaction point. Figure 6 demonstrates the principle of this method for

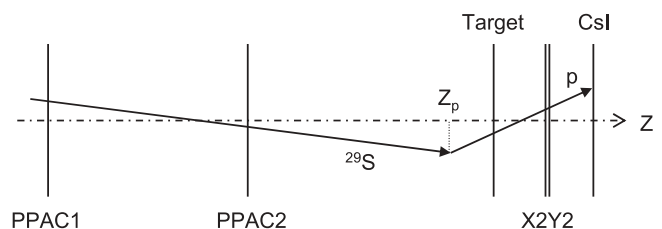


FIG. 6. Sketch of the cross-point-of-trajectories method to determine the reaction point for a $1p$ event. See text for details.

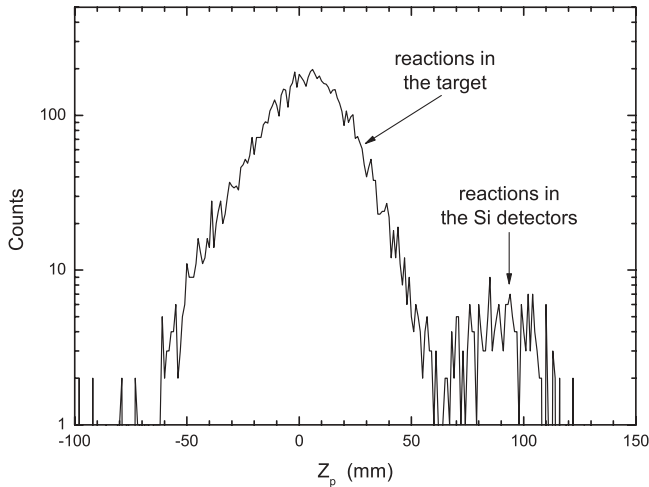


FIG. 7. Z position of the reaction points for $1p$ events. Reactions in the target and in the Si detectors are clearly separated.

a $1p$ emission. The cross-point of two trajectories represents the actual interaction point, and its Z position can be easily deduced mathematically. In the first instance, $1p$ events with high statistics were utilized to check the effectiveness of this method, as shown in Fig. 7. Here, the $1p$ events stand for $^{29}\text{S} \rightarrow ^{28}\text{P} + p$ coincident events. Two components can be seen in the figure. One locates around $Z_p \simeq 0$ mm with the range from -50 mm to 50 mm, originating from the reactions in the target. Another one with the range from 65 mm to 120 mm results from the reactions in the Si detectors, including SSSDs and the large area silicon detectors. The resolution of the Z position, which is mainly under the influence of the size of the CsI detector unit, was estimated as 50 mm. Although the position resolution is not so good, it is enough to separate the reactions in the target from the reactions in other materials, due to the large distance separation in the experimental setup.

Later, the cross-point-of-trajectories method was applied to determining the reaction points of $2p$ events. Figure 8 shows the spectrum of Z_{p1} versus Z_{p2} , where the trajectories of $p1$ and $p2$ were tracked individually. Only the events of both Z_{p1} and Z_{p2} within ± 50 mm were accepted as the effective interactions in the target, as shown by the square in the figure.

E. Selection procedure

First, the ^{29}S beam was selected on the ΔE -ToF spectrum (Fig. 2). Second, the $2p$ events that appeared inside the gate on the double-hit D2-CsI spectrum (bottom panel of Fig. 5) were chosen. Third, the selected events were further purified by the Si-isotope gate on the Y1-X1 spectrum (Fig. 3) and the time window on the ToF-Y1 versus ToF spectrum (Fig. 4). Thus, the accidentally coincident events such as the $^{26,27}\text{Si}$ directly from the secondary beams were ruled out. Moreover, the gate on the Z_{p1} versus Z_{p2} spectrum was added to make sure of the reactions in the target and to pick out the reactions in other layers. Finally, only about 400 effective ^{27}Si - p - p events passed through the above strict selection.

III. EXPERIMENTAL RESULTS

Once the ^{27}Si - p - p event is determined, the relative momentum ($q_{pp} = |\mathbf{p}_1 - \mathbf{p}_2|/2$), the opening angle ($\theta_{pp}^{c.m.}$, in the center of mass system of ^{29}S), and the relative energy (E_{pp}) of two protons, as well as the invariant mass of final three-body system, can be deduced, event-by-event, by the relativistic-kinematics reconstruction under the constraints of energy and momentum conservation.

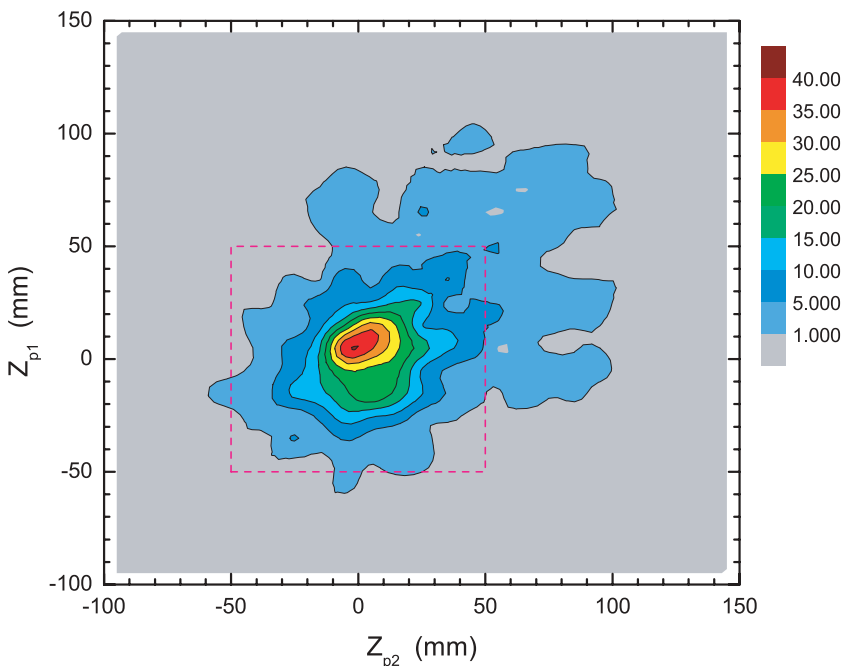


FIG. 8. (Color online) Two-dimensional plot of the Z position of the reaction points for $2p$ events. The square shows the gate for selecting the effective interactions in the target.

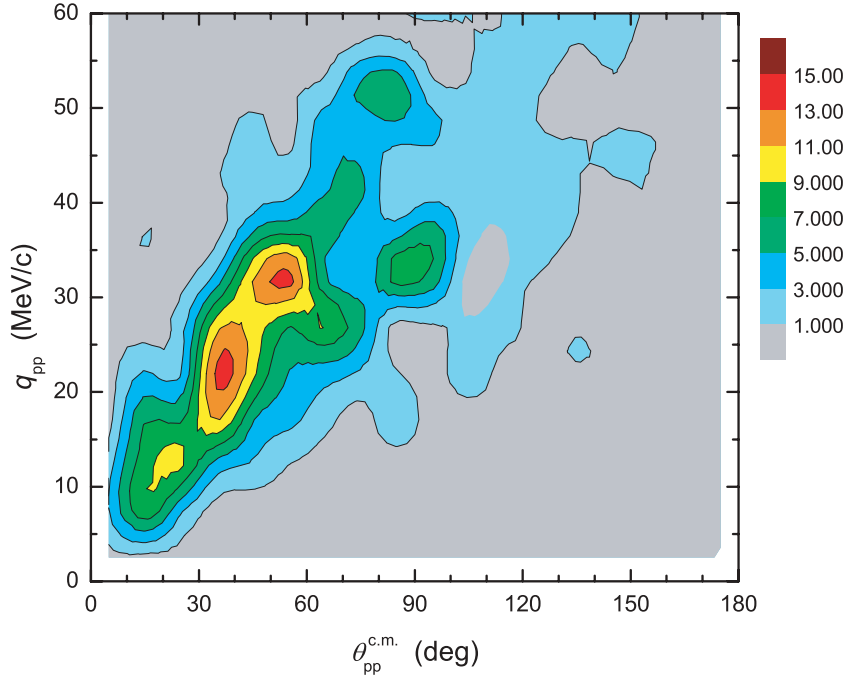


FIG. 9. (Color online) The spectrum of q_{pp} versus $\theta_{pp}^{c.m.}$ for all the ^{27}Si - p - p coincident events. Two obvious peaks appear at (35, 22.5) and (55, 32.5), indicating the strong p - p correlations.

A. Relative momentum and opening angle

The particular case of ^2He cluster decay is currently of interest. For ^2He cluster emission, the most prominent feature is the enhanced peak around $q_{pp} = 20$ MeV/ c due to the strong attractive nuclear interaction in the singlet s wave when two protons emit at close proximity in space and time [30–32]. Another striking feature is that the opening angle, which depends on the decay energy and the binding energy of $2p$, is smaller than 90° in the center of mass system. Figure 9 shows the spectrum of q_{pp} versus $\theta_{pp}^{c.m.}$ for all the ^{27}Si - p - p coincident events. Two obvious peaks appear at the positions of $(\theta_{pp}^{c.m.}, q_{pp}) = (35, 22.5)$ and $(55, 32.5)$. The small $\theta_{pp}^{c.m.}$ combined with small q_{pp} indicate the strong p - p correlations. However, for the three-body democratic decay, the $\theta_{pp}^{c.m.}$ and q_{pp} may have the similar behaviors due to the final state interaction (FSI) [6]. A rigorous theoretical treatment is required to make these behaviors clear. This area is worthy of further study.

B. Emission from different excitation regions

It is necessary to know the decay energy in the study of $2p$ emission mechanisms. To this end, the excitation-energy spectrum of ^{29}S was deduced from the invariant mass of the three-body system of $^{27}\text{Si} + p + p$, as shown in Fig. 10. Two conspicuous peaks appear at $E_x = 7.4$ and 10.0 MeV, which indicate some resonant states close to the top of the Coulomb barrier. Unfortunately, the energy levels and their spin-parities are still unknown for this nucleus. Only this invariant mass spectrum can be used at present. Considering the energy and position resolutions of the detector array, the experimental excitation-energy resolution was estimated as 400 keV. So the energy bin of ± 400 keV was selected to study the q_{pp} and $\theta_{pp}^{c.m.}$ for different excitation-energy regions.

To make a comparison, two typical excitation-energy regions, $7.0 \leq E_x \leq 7.8$ MeV and $9.6 \leq E_x \leq 10.4$ MeV, were chosen to study in detail. The q_{pp} and $\theta_{pp}^{c.m.}$ distributions for these two regions are shown in Figs. 11 and 12, respectively. For the region of $7.0 \leq E_x \leq 7.8$ MeV, the experimental data show a maximum at $q_{pp} = 35$ MeV/ c and a nearly symmetric distribution around $\theta_{pp}^{c.m.} = 90^\circ$. But for the region of $9.6 \leq E_x \leq 10.4$ MeV, an enhanced peak appears at $q_{pp} = 20$ MeV/ c and the opening angles reach the maximum at 35° . The MC simulations, in which the geometry of the detector arrangement was taken into account, were carried out to investigate the decay mechanism. The fragment angular distributions were calculated by the process of diffraction dissociation [33] and then sampled for simulations. Thus the deflections introduced by the Coulomb and nuclear force were taken into account. For the ^2He cluster decay, the p - p

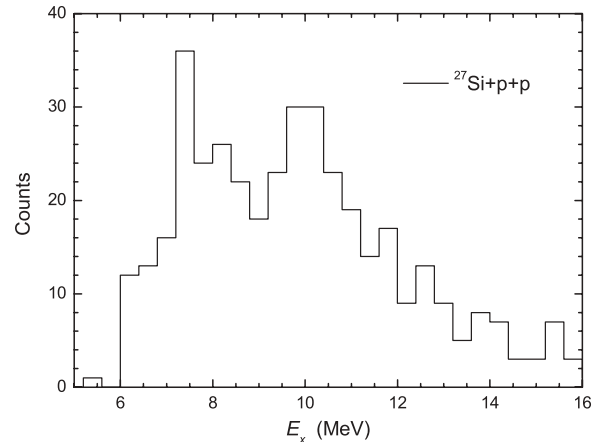


FIG. 10. Excitation-energy spectrum of ^{29}S reconstructed from $^{27}\text{Si} + p + p$ events.

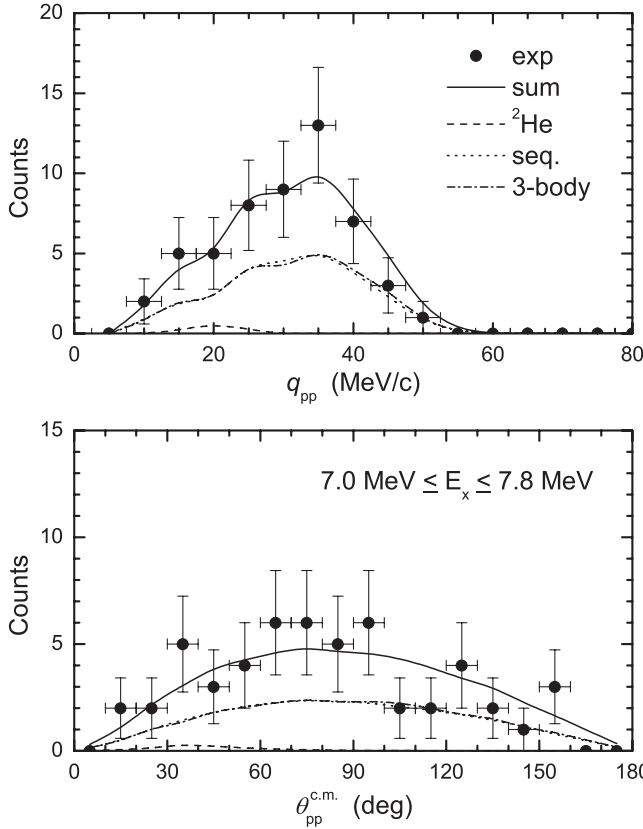


FIG. 11. The relative momentum and opening angle of two protons for the states of $7.0 \leq E_x \leq 7.8$ MeV. No obvious ${}^2\text{He}$ cluster decay was observed.

resonant energy was assumed to be 0.4 MeV with ± 0.2 MeV in width. Unfortunately, the strict calculation for the decay mechanism is impossible because the configurations of initial, intermediate, and final states are still unavailable. For the sake of simplification, the $2p$ emissions were treated as the extreme decay modes like ${}^2\text{He}$ cluster emission, three-body phase-space decay, and two-body sequential emission. And then samplings were made in the two-body or three-body phase-space. The spins and orbital momenta were omitted, and the FSI was consequently neglected. It should be pointed out that the q_{pp} and $\theta_{pp}^{c.m.}$ distributions for the two-body sequential decay and the three-body phase-space decay are almost identical because of the existence of large amounts of intermediate states and final states in the daughter and granddaughter nuclei, respectively. Therefore their branching ratios were taken as the same value. The experimental results were well reproduced by the MC simulations, see the dashed, dash-dotted, and dotted curves shown in Figs. 11 and 12 for the ${}^2\text{He}$ cluster, three-body phase-space, and two-body sequential decays, respectively. The solid curves are the sum of the above three components. The branching ratio of ${}^2\text{He}$ cluster decay from the $9.6 \leq E_x \leq 10.4$ MeV states was determined as $29^{+10}_{-11}\%$ by fitting the experimental data. The upper and lower limits were deduced by χ^2 analysis. The branching ratios of ${}^2\text{He}$ cluster decay were less than 10% for the $7.0 \leq E_x \leq 7.8$ MeV states, and also for other states that are not presented here.

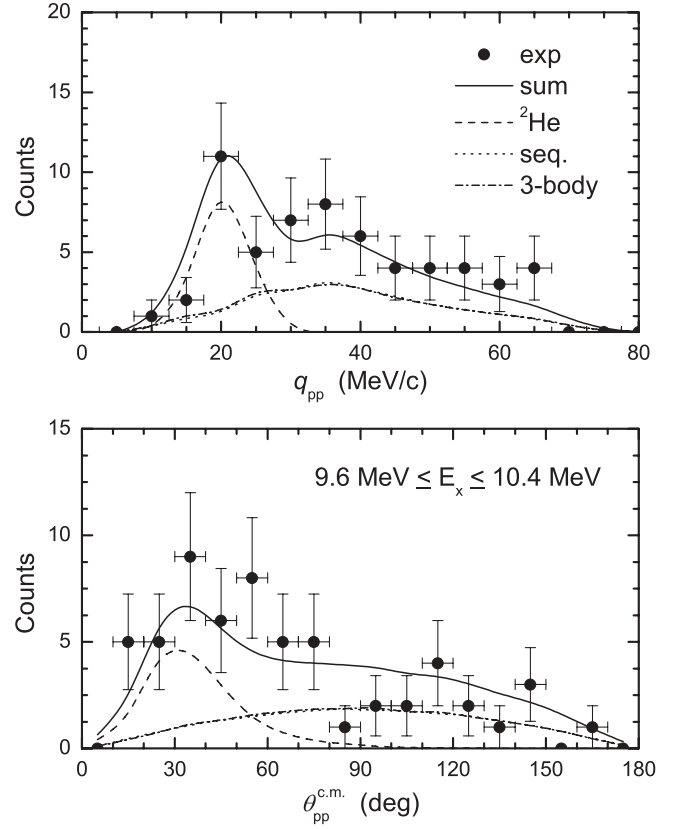


FIG. 12. Same as Fig. 11, but for the states of $9.6 \leq E_x \leq 10.4$ MeV. Obvious ${}^2\text{He}$ cluster decay with a branching ratio of $29^{+10}_{-11}\%$ was observed.

C. Relative energy

The $2p$ relative energy may carry some useful information on decay mechanisms. Figure 13 illustrates the E_{pp} spectra of $2p$ emissions from the $9.6 \leq E_x \leq 10.4$ MeV (solid line) and $7.0 \leq E_x \leq 7.8$ MeV (dashed line)

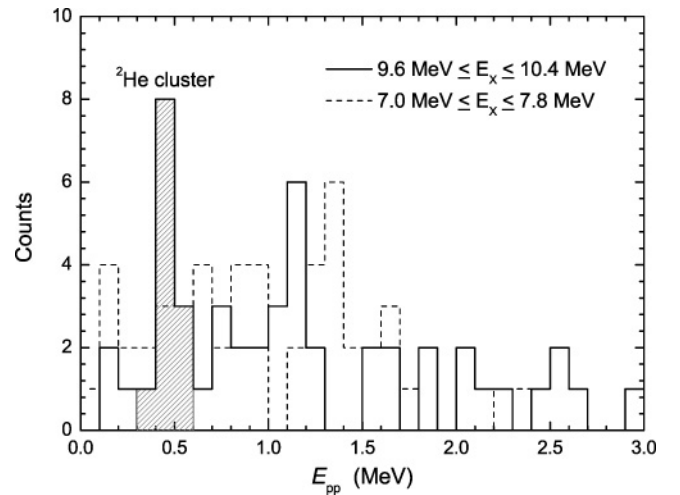


FIG. 13. The relative energy of two protons emitted from the $9.6 \leq E_x \leq 10.4$ MeV (solid line) and $7.0 \leq E_x \leq 7.8$ MeV (dashed line) states of ${}^{29}\text{S}$. The shadow area shows the events with $15 \leq q_{pp} \leq 25$ MeV from the $9.6 \leq E_x \leq 10.4$ MeV states.

states, respectively. An enhanced peak appears at 0.45 MeV for the $9.6 \leq E_x \leq 10.4$ MeV states, but none appears for other states. To make clear its origin, the events of $2p$ emitted from the $9.6 \leq E_x \leq 10.4$ MeV states with $15 \leq q_{pp} \leq 25$ MeV/ c were cut and are shown in the figure by the shadow area. It indicates that the enhanced peak result from the component of q_{pp} around 20 MeV/ c , which may imply the ${}^2\text{He}$ cluster decay. The similar phenomenon was also mentioned in Ref. [20] for the deformed nucleus ${}^{94}\text{Ag}^m$. However, no preferential direction is favored in the process of ${}^{29}\text{S} \rightarrow {}^{27}\text{Si} + 2p$ because of the near-spherical core and the near-symmetric Coulomb barrier. The observed correlations may relate to the p - p correlations inside a nucleus, i.e., the ${}^2\text{He}$ cluster formation.

IV. SUMMARY

In summary, the decay mechanisms of two protons from the excited states populated by a ${}^{29}\text{S}$ beam bombarding a ${}^{197}\text{Au}$ target via Coulomb excitation have been investigated in an experiment by means of complete-kinematics measurements. The ${}^{27}\text{Si}$ - p - p coincident events were picked out under a strict selection procedure. The relative momentum, opening angle, and relative energy of two protons, as well as the invariant mass of the final system, were deduced by the relativistic-kinematics reconstruction of these events. The $2p$ events with small relative momenta and small opening angles were observed in the experiment, indicating the strong p - p correlation. The results were analyzed in a simple schematic model, in which

the extreme decay modes like ${}^2\text{He}$ cluster emission, three-body phase-space decay, and two-body sequential emission were taken into account. In the present status, the MC simulations show that $2p$ events emitted from the excitation region of $9.6 \leq E_x \leq 10.4$ MeV of ${}^{29}\text{S}$ exhibit the feature of ${}^2\text{He}$ cluster decay with a branching ratio of $29_{-11}^{+10}\%$. But no obvious signatures of ${}^2\text{He}$ cluster decay were found for other regions. More statistics are needed to reduce the experimental error. The present excitation-energy levels of ${}^{29}\text{S}$ are determined by the invariant mass spectrum and may not be so precise. High-quality measurement combined with the high-efficiency γ detector array is required to detect the energy levels and their configurations. The present work supports the idea [5,25,26] that $2p$ halo/skin may induce a large probability for direct $2p$ emission, especially at high excited states close to the top of the Coulomb barrier. Hence, one may imagine that the direct $2p$ decay, including the particular ${}^2\text{He}$ cluster decay, might be a familiar phenomenon when the two protons are close to the threshold and loosely bounded by the core. Certainly, more convincing experimental data are needed to support this idea.

ACKNOWLEDGMENTS

We thank the staff of HIRFL-RIBLL for supplying good quality beams. This work was supported by the National Natural Science Foundation of China under Grants 10675169, 10735100, and 10727505 and by the Major State Basic Research Developing Program under Grant 2007CB815003.

-
- [1] V. I. Goldansky, Nucl. Phys. **19**, 482 (1960).
 - [2] V. I. Goldansky, Nucl. Phys. **27**, 648 (1961).
 - [3] S. Hofmann, W. Reisdorf, G. Mützenber, F. P. Heßberger, J. R. H. Schneider, and P. Armbruster, Z. Phys. A **305**, 111 (1982).
 - [4] O. Klepper, T. Batsch, S. Hofmann, R. Kirchner, W. Kurcewicz, W. Reisdorf, E. Roeckl, D. Schardt, and G. Nyman, Z. Phys. A **305**, 125 (1982).
 - [5] B. Blank and M. Płoszajczak, Rep. Prog. Phys. **71**, 046301 (2008), and references therein.
 - [6] O. V. Bochkarev, L. V. Chulkov, A. A. Korshennikov, E. A. Kuzmin, I. G. Mukha, and G. B. Yankov, Nucl. Phys. **A505**, 215 (1989).
 - [7] D. F. Geesaman, R. L. McGrath, P. M. S. Lesser, P. P. Urone, and B. VerWest, Phys. Rev. C **15**, 1835 (1977).
 - [8] M. Pfützner, E. Badura, C. Bingham *et al.*, Eur. Phys. J. A **14**, 279 (2002).
 - [9] J. Giovannazzo, B. Blank, M. Chartier *et al.*, Phys. Rev. Lett. **89**, 102501 (2002).
 - [10] J. Giovannazzo, B. Blank, C. Borcea *et al.*, Phys. Rev. Lett. **99**, 102501 (2007).
 - [11] K. Miernik, W. Dominik, Z. Janas *et al.*, Phys. Rev. Lett. **99**, 192501 (2007).
 - [12] B. Blank, A. Bey, G. Canchel *et al.*, Phys. Rev. Lett. **94**, 232501 (2005).
 - [13] J. Gómez del Campo, A. Galindo-Uribarri, J. R. Beene *et al.*, Phys. Rev. Lett. **86**, 43 (2001).
 - [14] G. Raciti, G. Cardella, M. De Napoli, E. Rapisarda, F. Amorini, and C. Sfienti, Phys. Rev. Lett. **100**, 192503 (2008).
 - [15] A. Azhari, R. A. Kryger, and M. Thoennessen, Phys. Rev. C **58**, 2568 (1998).
 - [16] M. J. Chromik, B. A. Brown, M. Fauerbach, T. Glasmacher, R. Ibbotson, H. Scheit, M. Thoennessen, and P. G. Thirolf, Phys. Rev. C **55**, 1676 (1997).
 - [17] M. J. Chromik, P. G. Thirolf, M. Thoennessen, B. A. Brown, T. Davinson, D. Gassmann, P. Heckman, J. Prisciandaro, P. Reiter, E. Tryggestad, and P. J. Woods, Phys. Rev. C **66**, 024313 (2002).
 - [18] T. Zerguerras, B. Blank, Y. Blumenfeld *et al.*, Eur. Phys. J. A **20**, 389 (2004).
 - [19] C. Dossat, A. Bey, B. Blank *et al.*, Phys. Rev. C **72**, 054315 (2005).
 - [20] I. Mukha, E. Roeckl, L. Batist *et al.*, Nature (London) **439**, 298 (2006).
 - [21] I. Mukha, K. Sümmerer, L. Acosta *et al.*, Phys. Rev. Lett. **99**, 182501 (2007).
 - [22] I. Mukha, L. Grigorenko, K. Sümmerer *et al.*, Phys. Rev. C **77**, 061303(R) (2008).
 - [23] B. Q. Chen, Z. Y. Ma, F. Grümmer, and S. Krewald, J. Phys. G **24**, 97 (1998).
 - [24] C. J. Lin, H. Q. Zhang, Z. H. Liu, Y. W. Wu, F. Yang, and M. Ruan, Phys. Rev. C **66**, 067302 (2002).
 - [25] R. Kanungo, M. Chiba, S. Adhikari *et al.*, Phys. Lett. **B571**, 21 (2003).
 - [26] L. V. Grigorenko, Yu. L. Parfenova, and M. V. Zhukov, Phys. Rev. C **71**, 051604(R) (2005).

- [27] Liu Zu-Hua, Ruan Ming, Zhao Yao-Lin *et al.*, *Chin. Phys. Lett.* **21**, 1711 (2004).
- [28] C. J. Lin, X. X. Xu, G. L. Zhang *et al.*, *AIP Conf. Proc.* **961**, 117 (2007).
- [29] Z. Sun, W.-L. Zhan, Z.-Y. Guo, G. Xiao, and J.-X. Li, *Nucl. Instrum. Methods Phys. Res. A* **503**, 496 (2003).
- [30] S. E. Koonin, *Phys. Lett.* **B70**, 43 (1977).
- [31] W. G. Lynch, C. B. Chitwood, M. B. Tsang *et al.*, *Phys. Rev. Lett.* **51**, 1850 (1983).
- [32] M. A. Bernstein, W. A. Friedman, W. G. Lynch *et al.*, *Phys. Rev. Lett.* **54**, 402 (1985).
- [33] A. G. Sitenko, A. D. Polozov, M. V. Evlanov, and A. M. Sokolov, *Nucl. Phys.* **A442**, 122 (1985).